LiFSA and Urea/Dimethylurea Eutectic Electrolytes for Lithium Metal Batteries

ACS APPLIED ENERGY MATERIALS

www.acsaem.org

Article

LiFSA and Urea/Dimethylurea Eutectic Electrolytes for Lithium Metal Batteries

Nanako Ito,[‖] Tomooki Hosaka,*[,‖] Mirna Alhanash, Teppei Furuichi, Ryoichi Tatara, Zachary T. Gossage, Patrik Johansson, and Shinichi Komaba*

Cite This: https://doi.org/10.1021/acsaem.5c02275

Read Online

ACCESS | Metrics & More | Article Recommendations | Supporting Information

ABSTRACT: Eutectic electrolytes are attracting increasing attention as liquid electrolytes for secondary batteries as they are potentially lower cost, less/nonflammable, and more environmentally benign than the current state-of-the-art. We have successfully developed eutectic electrolytes combining the $LiN(SO_2F)_2$ (LiFSA) with urea and dimethyl urea and investigated the physicochemical properties, solution structures, and applicability of these binary and ternary melts to lithium batteries. Solution structure analysis and electrochemical measurements suggest that reducing free solvent enhances anodic stability, while mitigating solvent clustering through hydrogen bonding improves cathodic stability. Moreover, LiFSA concentrated electrolytes of LiFSA/urea/dimethylurea (1:1:1) and LiFSA/dimethylurea (1:2) exhibited excellent compatibility with lithium metal due to the formation of an organic−inorganic hybrid solid electrolyte interphase. These electrolytes enable the reversible plating and stripping of lithium metal, as well as the stable operation of 4 V-class lithium metal batteries.

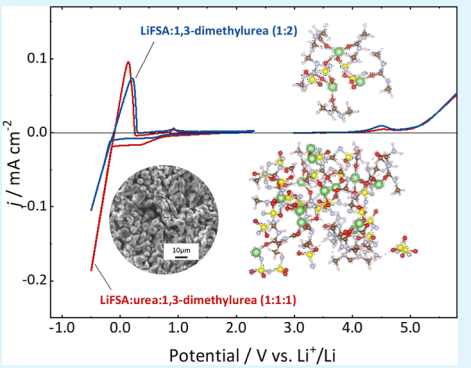

KEYWORDS: *lithium-ion battery, lithium metal battery, deep eutectic solvent, electrolyte, solid-electrolyte interphase*

INTRODUCTION

Lithium-ion batteries (LIBs) remain in high demand as power sources for portable electronic devices, electric vehicles, and other applications due to their high voltage and energy density.[1] At the same time, there is significant interest in further improving the energy density of LIBs by replacing the graphite negative electrode with lithium metal, referred to as lithium metal batteries (LMBs).[2] While graphite is a highly reliable material for alkali-ion batteries,[3] the ultrahigh capacity (3860 mAh g^{-1}) and very low redox potential (−3.04 V vs SHE) of lithium metal make it the most promising negative electrode material for next-generation batteries.[4] However, the high reactivity of lithium metal presents a significant safety issue, particularly when combined with the flammable organic electrolytes (e.g., based on carbonate solvents) used in commercial batteries.[5] Furthermore, LMBs have additional issues such as low Coulombic efficiency (CE) and dendrite growth,[6] problems which are also linked to the electrolyte.[7,8] Consequently, significant research is focused on developing safe and reliable electrolytes, including solid-state electrolytes,[9,10] flame-retardant organic electrolytes (e.g., trimethyl phosphate-based electrolyte),[11−13] highly concentrated organic electrolytes,[14,15] and ionic liquids (ILs). While solid-state electrolytes offer an attractive solution, maintaining effective solid/solid interfaces remains challenging due to the enormous volume changes of the Li metal anode during cycling. Flame-retardant liquid electrolytes also present limitations, including the toxicity of organic solvents and organic cations, as well as high costs. Consequently, researchers have focused on developing electrolytes that substitute the solvents with flame-retardant, nontoxic, and cost-effective alternatives.[16] Aqueous electrolytes represent one promising approach for LIBs,[16,17] but their application in LMBs is limited by water's inherently low reduction stability.

Recently, eutectic electrolytes or deep eutectic electrolytes (DEEs) have been recognized as potential nonflammable electrolytes for LIBs,[18−20] sodium-ion batteries (SIBs),[21] LMBs,[22] and sodium metal batteries (SMBs).[23,24] DEEs can be prepared from low-cost, safe, and nontoxic components, such as choline chloride, urea, and carboxylic acids.[25,26] By combining these hydrogen bond donors (HBDs) with acceptor compounds (or a Lewis base/acid combination), a deep freezing point depression occurs, enabling the use of low-volatile and low-flammable solid organic compounds as "solvents".[27] While DEEs can achieve low flammability due to their low volatility,[28,29] some issues remain, such as low discharge capacities and retention, and poor CE, probably

Received: July 23, 2025
Revised: December 12, 2025
Accepted: December 16, 2025

originating from their protic nature. Protic solvents can cause hydrogen evolution on low-potential negative electrodes, and therefore, promoting passivation through a stable solid electrolyte interphase (SEI) formation is key to attain high capacity retention.[20,30,31]

In a previous work, some of us reported on binary DEEs prepared from urea derivatives and lithium bis(fluorosulfonyl)-amide (LiFSA). We mainly used urea and 1,3-dimethyl urea (DMU) as they are both nontoxic and cost-effective (~80 $/kg, reagent grade), especially as compared to alternative solvents such as ethylene carbonate (~2000 $/kg) and *N*-ethyl-*N*-methylpyrrolidinium bis(trifluoromethanesulfonyl)-amide (29,960 $/kg). Moreover, we found differences in the SEI, CE of positive and negative electrodes, and electrochemical stability windows (ESWs).[32] Specifically, an LiFSA/urea (1:4) electrolyte enabled stable cycling of $Li_4Ti_5O_{12}$ (LTO) via a urea-derived, organic-rich SEI. In contrast, an electrolyte of LiFSA and 1,3-dimethylurea at the same concentration failed to stabilize the LTO electrode. However, the asymmetric structure of DMU enabled the preparation of a highly concentrated electrolyte, LiFSA/DMU (1:2), which yielded a higher CE for LTO electrodes due to the formation of an inorganic-rich SEI.

Although our previous study indicates that the choice of urea derivative is critical to electrochemical performance, the impact of its molecular structure on the solution environment and the resulting electrochemical stability is not fully understood, partly due to the narrow liquid-phase range of the LiFSA−urea system. Furthermore, the application of these DEEs to LMBs has not yet been demonstrated. Therefore, this study investigates the solution structures of binary and ternary DEEs (TDEEs) and evaluates their applicability to LMBs to better understand the role of different HBDs.

EXPERIMENTAL SECTION

Electrolyte Preparation

(T)DEEs were prepared by mixing various molar ratios of LiFSA (≥99%, Kishida Chemical) and urea derivatives at 25 ± 5 °C for ~10 h in an Ar-filled glovebox (dew point = −70 °C). Urea (≥99.0%, Wako Pure Chemical Industries) and dimethylurea (≥98%, Tokyo Chemical Industry) were used as purchased without further purification or drying. This is primarily due to the limitations caused by the sublimation and thermal decomposition of urea.

Electrode Preparation

The positive electrodes consisted of 80 wt % $LiMn_2O_4$ (LMO) (Toshima Manufacturing), 10 wt % conductive carbon, and 10 wt % polyvinylidene fluoride (PVdF, #9100, Kureha). Acetylene black (AB, Li-400, Denka) was used as the conductive carbon for all battery electrodes. The electrodes were prepared by casting the mixture slurry with *N*-methylpyrrolidone (NMP) onto Ti foil with a doctor blade and drying at 80 °C under a vacuum. The average thickness of the coating layer was ca. 17 μm. Activated carbon electrodes were prepared with 80 wt % activated carbon (YP50F, Kuraray), 10 wt % Ketjen Black (KB, Carbon ECP, Lion), and 10 wt % polytetrafluoroethylene (PTFE, Daikin) on a Ti mesh and dried at 100 °C. The mass loading of LMO in the electrodes was in the range of 1.6−2.1 mg cm^{-2}.

Electrochemical Characterization

Linear sweep voltammetry (LSV) and cyclic voltammetry (CV) were conducted using a three-electrode cell (SB1A, EC FRONTIER) with Pt foil (anodic scan) or Cu foil (cathodic scan) as a working electrode, an activated carbon counter electrode (>10 mg cm^{-2}), and an Ag^+/Ag reference electrode. The reference electrode consisted of a fritted capillary containing 3 mM silver trifluoromethanesulfonate in LiFSA/urea (1:4) and Ag wire. The reference electrode potential vs $Li^+/Li°$ was calibrated in each electrolyte using the redox potential of LTO electrodes (1.55 V vs $Li^+/Li°$, Table S1). All LSV and CV were conducted at 0.5 mV s^{-1}. Galvanostatic charge−discharge tests were conducted using a 2032 coin cell with a Li metal counter electrode (200 μm thick, ca. 10 mg, Honjo Chemical) and glass fiber separator (GB-100R, Advantec, 380 μm thick) soaked with 100 μL of electrolyte. Measurements were conducted using a VMP3 (Biologic) instrument at 25 ± 5 °C without any preformation cycles. To ensure reproducibility, all measurements were performed on a minimum of three independent cells.

Electrolyte and Electrode Characterization

The glass transition temperature and melting point of our LiFSA/urea derivative (T)DEEs were analyzed using differential scanning calorimetry (DSC, NETZSCH DSC3500 Sirius) at a temperature scanning rate of 10 °C min^{-1}. The thermal stability was tested using a thermogravimetric analyzer (DTG-60, Shimadzu) at a scan rate of 10 °C min^{-1} in an Ar atmosphere. The ionic conductivities of the electrolyte solutions were measured using an ionic conductivity meter (CM-41X, TOA DKK) at 25 °C ± 0.1 °C. The ionic conductivity meter was calibrated using a conductivity standard solution (1413 μS cm^{-1}, Horiba). The standard deviation of three replicates was confirmed to be less than 2% using the standard solution. The viscosities of the electrolyte solutions were measured using a rolling ball viscometer (Lovis 2000 M/ME, Anton Paar) at 25 °C ± 0.005 °C. Solution structures of the (T)DEEs were analyzed using Raman spectroscopy (Raman-11, Nanophoton) with a 532 nm laser and at a resolution of 2.0 cm^{-1}. The samples were sealed in Ar-filled bottles. The Raman spectra were calibrated using the peak originating from silicon at 520 cm^{-1}. Fourier transform infrared (FT-IR) spectroscopy was conducted using an Alpha II (Bruker) with the attenuated total reflection (ATR) method inside a glovebox to avoid air exposure. The ionic conductivities of the (T)DEEs were measured using an ionic conductivity meter (CM-41X, TOA DKK). The viscosities of the (T)DEEs were measured using a rolling ball viscometer (Lovis 2000 M/ME, Anton Paar) at 25 °C.

X-ray photoelectron spectroscopy (XPS, VersaProbe II, ULVAC-PHI) using Al Kα radiation (1486.6 eV) was used to analyze the tested electrodes.

Computational Details

The GFN-xTB approach[33] was used to run molecular dynamics (MD) simulations, which were conducted with the xTB method[34] through CP2K.[35] GFN-xTB offers a favorable compromise between the efficiency of classical MD and the accuracy of DFT.[33] This approach has been successfully applied to liquid electrolytes and molecular materials.[36,37] The method has been validated for Li−salt electrolytes,[38] showing comparable structural descriptors to AIMD at significantly lower computational cost. In contrast, xTB is less reliable for certain condensed-phase solids and strongly correlated systems.[37,39] The initial geometry of the (T)DEEs was generated using Packmol,[40] a tool designed to create well-packed molecular configurations for MD simulations. Packmol arranges molecules in predefined regions while avoiding atomic overlaps, enabling the construction of boxes with properly distributed molecules.

The MD simulations of the five (T)DEEs of LiFSA/urea (1:4), LiFSA/DMU (1:2), LiFSA/DMU (1:4), LiFSA/urea/DMU (1:1:1), and LiFSA/urea (1:2) were conducted in cubic boxes with side lengths of 16.7 Å, 17.1 Å, 17.9 Å, 17.1 Å and 17.1 Å, respectively, and were made up of 504, 494, 594, 512, and 520 atoms, respectively.

The MD simulations were 100 ps each, with the first 40 ps being regarded as equilibration. The equilibration ran an *NPT* ensemble with 1 fs time-steps at 363 K and with the barostat set to 1 atm. A production run was then performed in the *NVT* ensemble using 1 fs time steps, with a Nosé−Hoover thermostat[41−43] maintaining a temperature of 363 K. The resulting trajectories were analyzed using VMD,[44] and the local structure was examined by computing the radial distribution functions (RDFs) using the pair distribution function $g(r)$. Integration of the RDF up to the first minima was performed to obtain the partial coordination numbers (pCNs). While simulations

https://doi.org/10.1021/acsaem.5c02275
ACS Appl. Energy Mater. XXXX, XXX, XXX−XXX

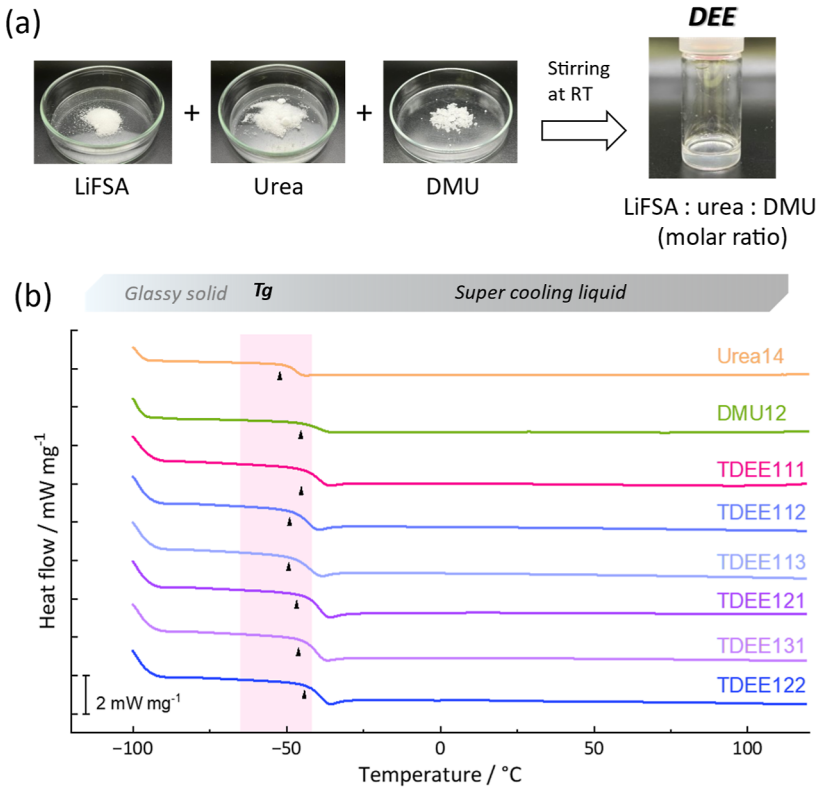

Figure 1. (a) Photograph of LiFSA, urea, DMU, and a resulting TDEE, and (b) DSC traces of (T)DEEs at a scan rate of 10 °C min^{-1}.

Table 1. Ionic Conductivity and Viscosity of Urea14 and DMU12, and the TDEEs

electrolyte name	composition (molar ratio)	ionic conductivity/mS cm^{-1}	viscosity/mPa s
Urea14	LiFSA/urea (1:4)	1.03	280.5 (7)
DMU12	LiFSA/DMU (1:2)	0.114	2533 (4)
TDEE111	LiFSA/urea/DMU (1:1:1)	0.174	1721 (4)
TDEE112	LiFSA/urea/DMU (1:1:2)	0.202	1411.0 (5)
TDEE113	LiFSA/urea/DMU (1:1:3)	0.226	940.1 (2)
TDEE121	LiFSA/urea/DMU (1:2:1)	0.346	997.8 (18)
TDEE131	LiFSA:/urea/DMU (1:3:1)	0.439	613.0 (7)
TDEE122	LiFSA/urea/DMU (1:2:2)	0.252	976.6 (4)

were conducted at 363 K to maintain the liquid state and enhance sampling, the analysis focuses on relative structural trends rather than direct comparison to room-temperature experiments.

RESULTS AND DISCUSSION

Physicochemical Properties

First, we investigated the phase stability of the TDEEs containing LiFSA, urea, and DMU. The TDEEs were prepared and analyzed using differential scanning calorimetry (DSC), and the results were compared with previously reported binary DEEs.[32] The TDEEs were stable, clear liquids at various molar ratios, including LiFSA/urea/DMU compositions of 1:1:1, 1:1:2, 1:2:1, 1:1:3, and 1:3:1 ratios (Figure 1a), henceforth denoted as TDEE111, TDEE112, etc. In addition, we have also tested some NaFSA or KFSA and urea binary mixtures. However, these are solid at 25 °C at both 1:2 and 1:4 ratios.

The DSC analysis revealed that these TDEEs, along with the binary DEEs LiFSA/urea (1:4) (Urea14) and LiFSA/DMU (1:2) (DMU12), all exhibit a glass transition temperature (T_g) of approximately −50 °C, with no other significant thermal events at higher temperatures (Figures 1b and S1). This indicates that they remain stable liquids at temperatures far below room temperature, with no notable phase separation or precipitation during heating and cooling cycles. However, the melting temperature (T_m) was difficult to observe in many compositions due to extremely slow crystallization, which made it impossible to determine the true eutectic points. Therefore, we shifted our focus to comparing TDEE111, TDEE122, and the binary DEEs for battery applications, as highly concentrated electrolytes have shown better electrochemical stability in previous studies.[23,28] Additionally, the DSC curves for all solutions lacked T_m above room temperature, confirming they exist as homogeneous liquids at room temperature. Moreover, urea-containing DEEs, including TDEEs, displayed a larger heat capacity step (ΔC_p) at the glass transition compared to DMU-based DEEs (Figure S2). This indicates a rapid increase in structural diversity and configurational entropy with rising temperature.[45,46] These observations can also correlate to the formation of hydrogen bonding[46] within urea-containing DEEs, which will be discussed later.

All TDEEs were found to be ionically conductive, with the ionic conductivity increasing and viscosity decreasing slightly along with higher urea content (Table 1). Furthermore, the

https://doi.org/10.1021/acsaem.5c02275
ACS Appl. Energy Mater. XXXX, XXX, XXX−XXX

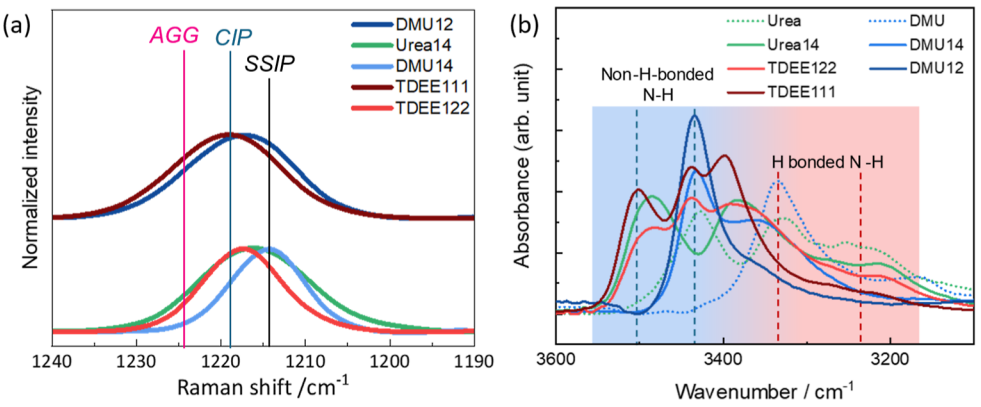

Figure 2. (a) Raman spectra in the range of 1190−1240 cm^{-1} and (b) FT-IR spectra in the range of 3100−3600 cm^{-1} of (T)DEEs.

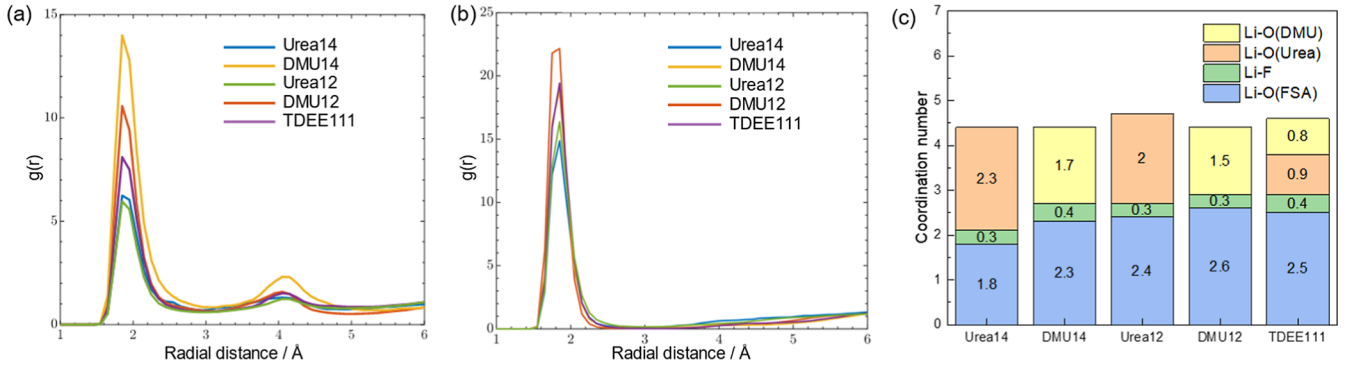

Figure 3. RDFs of (a) cation−anion Li^+−O (FSA) and (b) cation−solvent Li^+−O (Urea/DMU) interactions, and (c) pCNs of Li^+, in various (T)DEEs.

Walden plot shows that a higher urea content also resulted in greater ionicity, i.e., closer to the ideal KCl line (Figure S3), which can be attributed to a higher degree of LiFSA dissociation arising from the stronger interaction between Li^+ and urea. Thermogravimetric analysis also confirmed that these DEEs, particularly TDEE111, possess high thermal stability, showing minor weight loss (<5%) below 200 °C (Figure S4).

The standard error of viscosity was calculated based on four replicates. The data for Urea14 and DMU12 are taken from ref 32.

Solution Structures

To investigate the solution structures of the (T)DEEs, we used Raman spectroscopy, FT-IR spectroscopy, and MD simulations. Raman spectroscopy was used to probe the interactions involving the $[FSA]^-$ anion, as its S═O stretching peak is sensitive to both ionic coordination with Li^+ and hydrogen bonding with urea/DMU. The DMU14 electrolyte exhibits a peak around 1214 cm^{-1} with a shoulder at a higher wavenumber (Figure 2a). The main peak is in agreement with reported values for solvent-separated ion pairs (SSIPs), while the shoulder can be attributed to contact ion pairs (CIPs), which typically appear near 1218 cm^{-1}.[47] The TDEE122 and Urea14 electrolytes show broader peaks with a slight shift to higher wavenumbers, which may be due to increased CIP formation or direct hydrogen bonding between $[FSA]^-$ and urea (Figures S5 and S6a). As the LiFSA concentration increases, this peak shifts further (Figures 2a and S6b), indicating significant ion-pair formation, including CIPs and aggregates (AGGs), the latter of which are typically observed around 1224 cm^{-1}.[47] Overall, the Raman spectra suggest that mixing urea and DMU enhances ion-pair and/or hydrogen bond formation (Figures S5 and S6c).

FT-IR spectroscopy provided further insight into the hydrogen-bonding network through the N−H stretching bands. Peaks located at 3200−3350 cm^{-1} and 3400−3550 cm^{-1} can be assigned to H-bonded and non-H-bonded N−H groups, respectively (Figure 2b).[48] With increasing LiFSA concentration, the intensity of the H-bonded N−H peaks decreased while the non-H-bonded peaks increased, which is clearly illustrated in the difference spectra (Figure S7). Notably, for the DMU12 electrolyte, the intensity of H-bonded peaks was negligible.

These spectroscopic results indicate that as electrolyte salt concentration increases, solvent−solvent interactions are replaced by Li^+−solvent coordination. Furthermore, they confirm that DMU has low hydrogen bonding formation ability as compared to urea, as expected from its chemical structure.

MD simulations using the xTB method were conducted to illustrate the solution structure. The RDFs show a clear first solvation shell at ∼2 Å in both $[FSA]^-$ and urea/DMU (Figure 3a,b). A comparative analysis of the pCNs highlights relative differences in ion dissociation between the DEEs. In particular, the urea-based DEEs show enhanced ion dissociation, shown by smaller Li−O(FSA) and Li−F pCN values than for the DMU-based electrolytes at the same salt concentration (Figure 3c and Table S3), consistent with their higher measured ionicity.

The pCNs for Li−O(urea) and Li−O(DMU) were determined to be 2.3 and 1.7 in the Urea14 and DMU14 electrolytes, respectively (Figure 3c). These values are

https://doi.org/10.1021/acsaem.5c02275
ACS Appl. Energy Mater. XXXX, XXX, XXX−XXX

significantly lower than the value of 4 expected for a fully coordinated state, indicating that these electrolytes contain urea/DMU molecules that are not coordinated with Li^+ (i.e., "free" or hydrogen-bonded solvents) (Figure 3c and Table S4). In contrast, the more concentrated 1:2 electrolytes (DMU12, Urea12, and TDEE111) contained only a negligible amount of "free" solvent, as the pCN of urea/DMU is close to 2 (Figure 3c). Consistent with the Raman spectra, the simulations show that higher salt concentrations favor increased Li^+−anion contacts, indicating a greater likelihood of CIPs and AGG formation. In addition to concentration, the specific urea derivative also affects the amount of free solvent, and urea-based electrolytes show less "free" solvent than DMU-based ones.

These "free" solvents can interact with anions or other solvent molecules through hydrogen bonds. Indeed, a combined analysis of angular distribution functions (ADF) and RDF suggested that the geometric arrangements of N−H···O/F geometrical configurations were predominantly located in the region of H−O/F distances (~2.0 Å) and bond angles (>135°) typical of hydrogen bonding (Figure S8). This supports the presence of hydrogen bonding in these solutions and is consistent with the FT-IR spectra shown in Figure 2b. However, the continuous nature of this geometric distribution complicates the clear designation of hydrogen bonds. Consequently, it was not feasible to quantify the hydrogen bonding within each electrolyte based on geometric characteristics.

Overall, the spectroscopic results and MD simulations are qualitatively consistent, indicating significant ion-pair formation in the higher-concentration solutions. Moreover, solvent−solvent hydrogen bonds are largely replaced by Li^+−solvent coordination in highly concentrated electrolytes. Specifically, the DMU12 electrolyte exhibited the least pronounced hydrogen-bonding characteristics in the N−H bond vibration (Figure 2b).

Electrochemical Stability and LMB Performance

Prior to battery tests, the ESW of the electrolytes was examined through voltammetry. Comparing the electrolytes with a 1:4 LiFSA-to-urea/DMU ratio, a lower proportion of urea resulted in higher anodic stability (Figure 4). Since these dilute electrolytes contain "free" solvent molecules, this result indicates that free urea decomposes anodically at a lower potential than free DMU. The highly concentrated electrolytes, DMU12 and TDEE111, demonstrated superior anodic stability. This trend is fully consistent with the established principle in highly concentrated electrolytes where most solvent molecules are coordinated to Li^+.[49,50] Comparing these concentrated electrolytes, TDEE111 exhibited a suppressed anodic current than DMU12 (Figure S9), which is consistent with the smaller amount of free solvent obtained in MD.

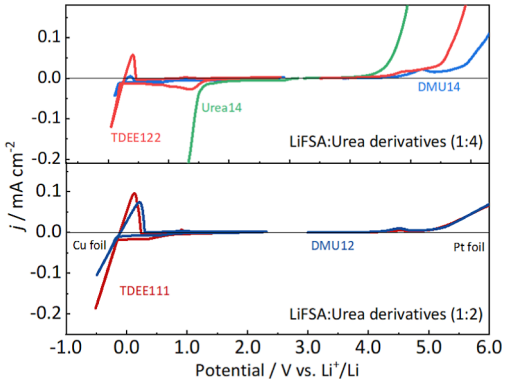

Figure 4. LSV and CV curves for (T)DEEs. The anodic and cathodic scans were conducted with Pt and Cu foil working electrodes, respectively.

During the cathodic scan using Cu foil as electrode, the Urea14 electrolyte showed a significant reduction current starting from approximately 1.4 V vs $Li^+/Li°$, which is attributed to continuous urea decomposition (Figures 4 and S10a). In contrast, TDEE122 demonstrated partially reversible lithium metal plating/stripping with a CE of 27% (Figures 4 and S10b). The low CE is mainly due to irreversible reactions below 1.0 V vs $Li^+/Li°$, which we again attribute to solvent decomposition. While DMU14 also showed a small redox couple for Li plating/stripping, its CE was very low (<1%) (Figures 4 and S10c).

Reversibility was significantly improved in the highly concentrated electrolytes. DMU12 and TDEE111 achieved a reasonable CE (~50%) from the second cycle onward, although minor solvent decomposition was still observed during the initial cycles, especially for TDEE111 (Figure S10d,e). The impact of solvent decomposition was more dominant in galvanostatic tests. The Li|DMU12|Cu cell demonstrated a CE of ~60%, whereas the Li|TDEE111|Cu cell showed a CE of only 24% (Figure S11a,b). Moreover, the DMU12 electrolyte achieved an average CE of ca. 79% over 10 cycles using a protocol proposed by Zhang et al.,[51] indicating better compatibility with Li−metal plating and stripping (Figure S11c).

Although water contamination in the electrolyte was suspected as a cause of irreversible capacity, no correlation was observed between the water content, as determined by Karl Fischer titration (Table S2), and the reductive stability or the CE of Li metal plating/stripping. Therefore, the irreversible reduction observed in the CV can be attributed to the reductive decomposition of urea or DMU, rather than water. Nevertheless, since the adverse effects of residual water decomposition cannot be ruled out, further improvements in electrochemical stability are expected through the ongoing optimization of the electrolyte's drying conditions.

The combined analysis of the solution structure and electrochemical stability reveals a correlation between hydrogen-bond formation and the side reactions observed during lithium metal plating and stripping. This is likely because hydrogen atoms in clustered, hydrogen-bonded solvents can readily dissociate to form hydrogen gas at low potential. Conversely, for isolated solvent molecules that are primarily coordinated to Li^+, the overpotential for the hydrogen evolution reaction is higher due to suppressed protonation.[52] This finding offers a critical insight: for protic eutectic electrolytes, disrupting solvent−solvent hydrogen bonding networks is essential for cathodic stability.

We further observe the tested Cu foil surface using SEM. After a constant potential application of −0.5 V vs $Li^+/Li°$ in TDEE111 (Figure S12a,b) for 5 h, which resulted in 1.33 mAh cm^{-2} capacity, the deposited film consisted of small bumpy lithium metal deposits (Figure 5a), in agreement with a previous report using a highly concentrated LiFSA electrolyte.[53] Round and small (5−10 μm in size) deposits are considered to be suitable for use in LMBs since there is little

https://doi.org/10.1021/acsaem.5c02275
ACS Appl. Energy Mater. XXXX, XXX, XXX−XXX

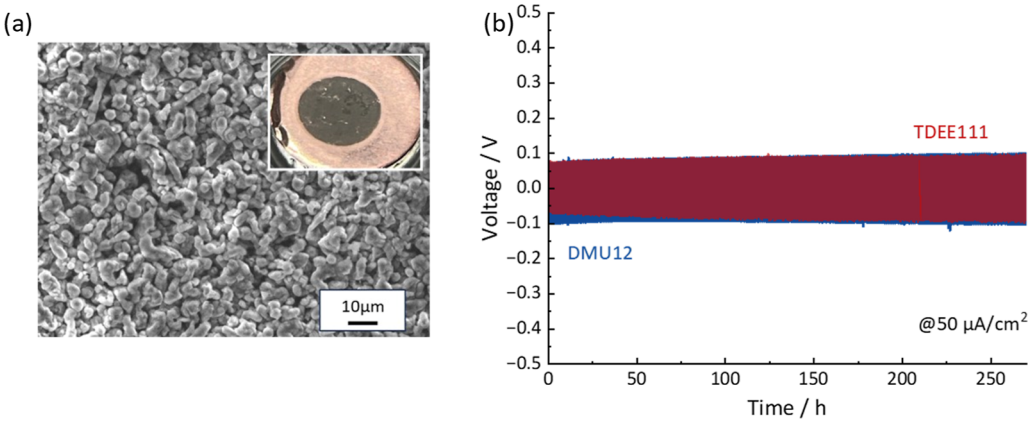

Figure 5. (a) SEM image of the surface/precipitate (lithium metal deposit) after constant potential deposition in TDEE111, and (b) voltage profiles of Li||Li symmetric cells with TDEE111 and DMU12 electrolytes at a current density of 50 μA cm^{-2}.

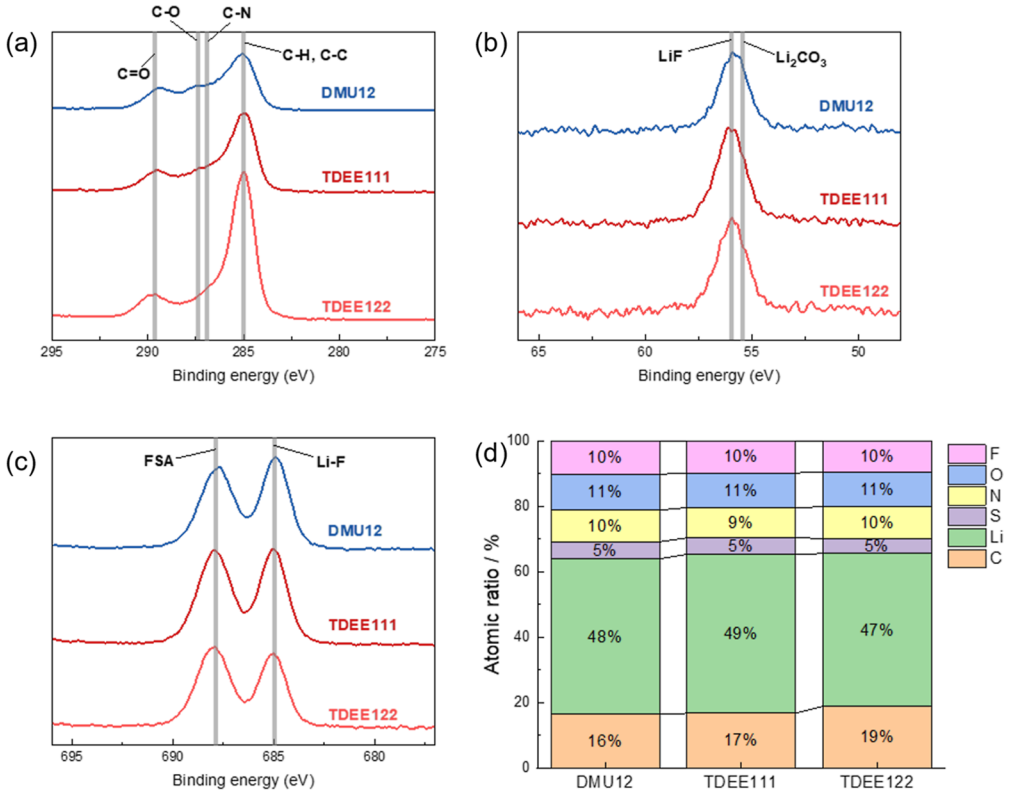

Figure 6. XPS spectra of lithium metal electrodes cycled in the symmetric Li||Li cells for 10 cycles. All spectra were normalized by the areal intensity of the corresponding N 1s spectra. (a) C 1s, (b) Li 1s, (c) F 1s, and (d) semiquantitative analysis of elements.

risk of penetration through the separator. Furthermore, EDS mapping shows that only a small amount of F and Cu exists on the surface, indicating that the Cu foil is almost entirely covered with lithium metal (Figure S12c−e). Further comparison of TDEE111 and DMU12 using the symmetric cell test showed that both were stable over 250 h, demonstrating excellent compatibility with lithium metal electrodes (Figure 5a). This is a noteworthy improvement in the applicability of DEEs to LMB cells, considering that a previously reported LiTFSA−urea-based DEE required the addition of a large amount (>50%) of fluoroethylene carbonate for the stable operation of 250 h.[22] Furthermore, both electrolyte cells maintained stable operation at current densities as high as 500 μA cm^{-2} without short-circuiting (Figure S13). At a higher current density of 1 mA cm^{-2}, however, all cells failed due to excessive overpotential.

Next, the SEI formed on the lithium metal electrodes was investigated using XPS after 10 cycles in symmetric Li||Li cells with the DMU12, TDEE111, and TDEE122 electrolytes. The resulting spectra showed only minor compositional differences. All electrodes displayed peaks assigned to C═O, C−O, and C−N functional groups in the C 1s, O 1s, and N 1s XPS spectra, confirming the presence of decomposition products from urea and/or DMU (Figure 6a). Furthermore, the Li 1s and F 1s spectra exhibited clear peaks assigned to LiF on all electrodes (Figure 6b,c). LiF is formed by decomposition of the FSA anion, which is enhanced by AGG formation.[54] The absence of a metallic Li peak suggests that the SEI is thicker

https://doi.org/10.1021/acsaem.5c02275
ACS Appl. Energy Mater. XXXX, XXX, XXX−XXX

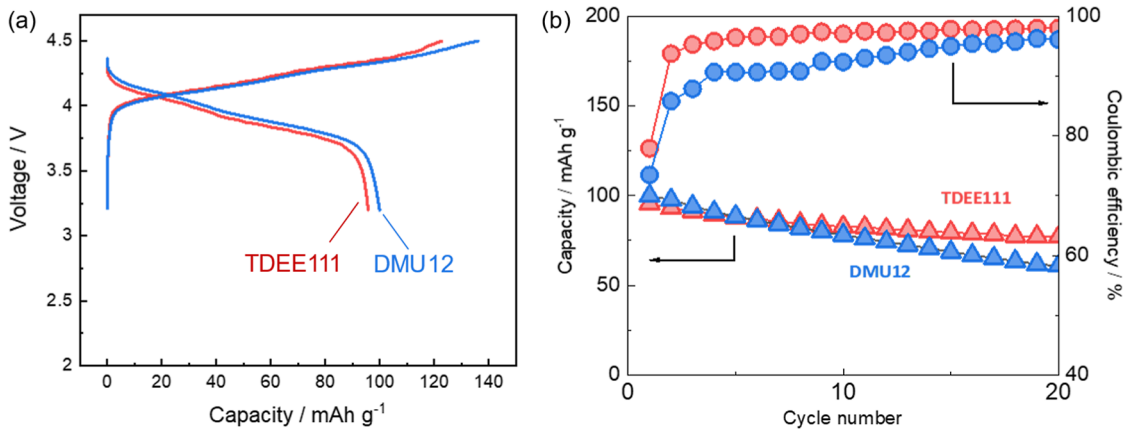

Figure 7. Charge−discharge curves of (a) Li ‖ Li_2MnO_4 cells using TDEE111 or DMU12 electrolytes at 30 mAh g^{-1}, and their (b) cycling performance and Coulombic efficiency.

than the detection depth of XPS (~5 nm). Therefore, the SEI composition may differ in deeper regions, necessitating future analysis with techniques like hard X-ray photoelectron spectroscopy.

Taken together, these results indicate the formation of an organic−inorganic hybrid SEI from all three (T)DEEs. A semi-quantitative analysis using elemental relative sensitivity factors revealed that the SEI formed in TDEE122 contained a higher atomic percentage of carbon than those formed in DMU12 and TDEE111, suggesting a greater degree of solvent decomposition. Nevertheless, the substantial variation in CE (e.g., 27% for TDEE122 and 45% for DMU12) appears to be governed not by the final SEI composition, but by the quantity of solvent consumed for the continuous formation and reconstruction of the SEI during cycling.

Finally, we evaluated the applicability of the (T)DEEs in LMBs using $LiMn_2O_4$ (LMO) positive electrodes. Cells with both the TDEE111 and DMU12 electrolytes showed reversible charge−discharge curves, delivering a capacity of approximately 100 mAh g^{-1} (based on the positive electrode active material mass) with an average operating voltage of 3.9 V. This performance demonstrates their suitability for 4 V-class lithium metal batteries (Figure 7a). The TDEE111 cell exhibited a higher CE than its DMU12 counterpart, which is consistent with its higher anodic stability as observed in the voltammetry experiments (Figure S9). Consequently, the TDEE111 cell achieved better cycling performance (Figure 7b). Nevertheless, the CE of the TDEE111 cell was still only approximately 98% even after 10 cycles, indicating that continuous electrolyte decomposition remains an issue. In addition, these cells retained only 40 mAh g^{-1} for TDEE111 and 20 mAh g^{-1} for DMU12 at a higher current density of 150 mA g^{-1} (Figure S14), which is likely due to the limited ionic conductivity (Table 1). Further optimization of the electrolyte composition and cell configuration, including electrolyte additives, diluents, and higher stack pressure, will improve long-term stability and rate capability.

CONCLUSIONS

In this study, we investigated binary and ternary mixtures of LiFSA, urea, and 1,3-dimethylurea (DMU) as (T)DEEs for lithium metal batteries. Compared to DMU, urea exhibits stronger coordination to Li^+ ions and a greater ability to act as a HBD toward anions and other urea molecules. This leads to a higher degree of LiFSA dissociation, fewer free solvent molecules, and more prominent solvent clustering in urea-based electrolytes. Our analysis suggests that reducing the amount of free solvent is essential for improving anodic stability, consistent with known effects in highly concentrated electrolytes. More importantly, mitigating solvent clustering is critical for enhancing cathodic stability. These factors can be controlled by creating ternary mixtures of urea and DMU. We found that a TDEE, LiFSA/urea/DMU (1:1:1), enables both reversible lithium metal plating and stripping and the stable cycling of a 4 V-class Li‖$LiMn_2O_4$ cell. This work not only presents a promising new electrolyte system but also provides a fundamental design rationale that can guide the future development of advanced eutectic electrolytes for next-generation batteries.

ASSOCIATED CONTENT

Supporting Information

The Supporting Information is available free of charge at https://pubs.acs.org/doi/10.1021/acsaem.5c02275.

Redox potential of LTO electrodes and calculated Li^+/Li° vs. Ag^+/Ag reference; Melting points (T_m) and glass transition points (T_g) of (a) LiFSA-urea, (b) LiFSA-1,3-DMU, and (c) LiFSA-urea-1,3-DMU (PDF)

DMU14_initial.xyz (XYZ)

DMU12_initial.xyz (XYZ)

TDEE111_initial.xyz (XYZ)

Urea12_initial.xyz (XYZ)

Urea14_initial.xyz (XYZ)

AUTHOR INFORMATION

Corresponding Authors

Tomooki Hosaka − *Department of Applied Chemistry, Tokyo University of Science, Shinjuku 162-8601, Japan; Department of Physics, Chalmers University of Technology, Gothenburg SE-41296, Sweden;* orcid.org/0000-0002-5922-8320; Email: hosaka@rs.tus.ac.jp

Shinichi Komaba − *Department of Applied Chemistry, Tokyo University of Science, Shinjuku 162-8601, Japan;* orcid.org/0000-0002-9757-5905; Email: komaba@rs.tus.ac.jp

https://doi.org/10.1021/acsaem.5c02275
ACS Appl. Energy Mater. XXXX, XXX, XXX−XXX

Authors

Nanako Ito − *Department of Applied Chemistry, Tokyo University of Science, Shinjuku 162-8601, Japan*

Mirna Alhanash − *Department of Physics, Chalmers University of Technology, Gothenburg SE-41296, Sweden*

Teppei Furuichi − *Department of Applied Chemistry, Tokyo University of Science, Shinjuku 162-8601, Japan*

Ryoichi Tatara − *Department of Applied Chemistry, Tokyo University of Science, Shinjuku 162-8601, Japan;* Present Address: Department of Chemistry and Life Science, Yokohama National University, Yokohama, 240-8501, Japan; orcid.org/0000-0002-8148-5294

Zachary T. Gossage − *Department of Applied Chemistry, Tokyo University of Science, Shinjuku 162-8601, Japan;* orcid.org/0000-0003-3745-2919

Patrik Johansson − *Department of Physics, Chalmers University of Technology, Gothenburg SE-41296, Sweden; Alistore-ERI, CNRS FR 3104, 80039 Amiens, Frances;* orcid.org/0000-0002-9907-117X

Complete contact information is available at: https://pubs.acs.org/10.1021/acsaem.5c02275

Author Contributions

[‖]N.I. and T.H. are contributed equally. T.H. and S.K. proposed the concept. N.I., T.F., and T.H. conducted experiments and analyses under the supervision of R.T., Z.G., and S.K. M.A. conducted MD simulations and analyses under the supervision of P.J. The manuscript was written through contributions of all authors. All authors have given approval to the final version of the manuscript.

Funding

MEXT Program: Data Creation and Utilization Type Materials Research and Development Project (JPMXP1122712807) JST-ASPIRE (JPMJAP2313) JST-CREST (JPMJCR21O6) JST-PRESTO (Grant No. JPMJPR2374) JSPS KAKENHI (JP20H02849, JP21K20561, JP22K14772, JP23K13829, and JP25H00905). Swedish Research Council (grants #2020-03988 and #2021-00613) VINNOVA/Batteries Sweden (BASE) (grant 2019-00064)

Notes

The authors declare no competing financial interest.

■ ACKNOWLEDGMENTS

This study was partially funded by the MEXT Program: Data Creation and Utilization Type Materials Research and Development Project (JPMXP1122712807), JST-ASPIRE (JPMJAP2313), JST-CREST (JPMJCR21O6), JST-PRESTO (Grant No. JPMJPR2374), and JSPS KAKENHI (JP20H02849, JP21K20561, JP22K14772, and JP23K13829), as well as the Swedish Research Council (grants #2020-03988 and #2021-00613) and VINNOVA/Batteries Sweden (BASE) (grant 2019-00064).

■ ABBREVIATIONS

CE, coulombic efficiency; AGG, aggregate; CIP, contact ion pair; CV, cyclic voltammetry; DEE, deep eutectic electrolyte; DMU, 1,3-dimethylurea; DSC, differential scanning calorimetry; EDS, energy-dispersive X-ray spectroscopy; FT-IR, Fourier-transform infrared spectroscopy; LIB, lithium-ion battery; LiFSA, lithium bis(fluorosulfonyl)amide; LMB, lithium−metal battery; LMO, lithium manganese oxide ($LiMn_2O_4$); LSV, linear sweep voltammetry; LTO, $Li_4Ti_5O_{12}$; MD, molecular dynamics; pCN, partial coordination number; RDF, radial distribution function; SEI, solid electrolyte interphase; SEM, scanning electron microscopy; SSIP, solvent-separated ion pair; TDEE, ternary deep eutectic electrolyte; T_g, glass transition temperature; XPS, X-ray photoelectron spectroscopy.

■ REFERENCES

(1) Li, M.; Lu, J.; Chen, Z.; Amine, K. 30 Years of Lithium-Ion Batteries. *Adv. Mater.* **2018**, *30* (33), 1800561.

(2) Asenbauer, J.; Eisenmann, T.; Kuenzel, M.; Kazzazi, A.; Chen, Z.; Bresser, D. The Success Story of Graphite as a Lithium-Ion Anode Material − Fundamentals, Remaining Challenges, and Recent Developments Including Silicon (Oxide) Composites. *Sustain. Energy Fuels* **2020**, *4* (11), 5387−5416.

(3) Gossage, Z. T.; Igarashi, D.; Fujii, Y.; Kawaguchi, M.; Tatara, R.; Nakamoto, K.; Komaba, S. New Frontiers in Alkali Metal Insertion into Carbon Electrodes for Energy Storage. *Chem. Sci.* **2024**, *15* (44), 18272−18294.

(4) Liu, B.; Zhang, J.-G.; Xu, W. Advancing Lithium Metal Batteries. *Joule* **2018**, *2* (5), 833−845.

(5) Xu, K. Nonaqueous Liquid Electrolytes for Lithium-Based Rechargeable Batteries. *Chem. Rev.* **2004**, *104* (10), 4303−4418.

(6) Liu, D.-H.; Bai, Z.; Li, M.; Yu, A.; Luo, D.; Liu, W.; Yang, L.; Lu, J.; Amine, K.; Chen, Z. Developing High Safety Li-Metal Anodes for Future High-Energy Li-Metal Batteries: Strategies and Perspectives. *Chem. Soc. Rev.* **2020**, *49* (15), 5407−5445.

(7) Feng, X.; Ouyang, M.; Liu, X.; Lu, L.; Xia, Y.; He, X. Thermal Runaway Mechanism of Lithium Ion Battery for Electric Vehicles: A Review. *Energy Storage Mater.* **2018**, *10*, 246−267.

(8) Tian, X.; Yi, Y.; Fang, B.; Yang, P.; Wang, T.; Liu, P.; Qu, L.; Li, M.; Zhang, S. Design Strategies of Safe Electrolytes for Preventing Thermal Runaway in Lithium Ion Batteries. *Chem. Mater.* **2020**, *32* (23), 9821−9848.

(9) Hamada, M.; Tatara, R.; Kubota, K.; Kumakura, S.; Komaba, S. All-Solid-State Potassium Polymer Batteries Enabled by the Effective Pretreatment of Potassium Metal. *ACS Energy Lett.* **2022**, *7* (7), 2244−2246.

(10) Ye, L.; Li, X. A Dynamic Stability Design Strategy for Lithium Metal Solid State Batteries. *Nature* **2021**, *593* (7858), 218−222.

(11) Zhang, X.-Q.; Cheng, X.-B.; Zhang, Q. Advances in Interfaces between Li Metal Anode and Electrolyte. *Adv. Mater. Interfaces* **2018**, *5* (2), 1701097.

(12) Liu, S.; Ji, X.; Piao, N.; Chen, J.; Eidson, N.; Xu, J.; Wang, P.; Chen, L.; Zhang, J.; Deng, T.; Hou, S.; Jin, T.; Wan, H.; Li, J.; Tu, J.; Wang, C. An Inorganic-Rich Solid Electrolyte Interphase for Advanced Lithium-Metal Batteries in Carbonate Electrolytes. *Angew. Chem., Int. Ed.* **2021**, *60* (7), 3661−3671.

(13) Wang, Z.; Wang, Y.; Li, B.; Bouwer, J. C.; Davey, K.; Lu, J.; Guo, Z. Non-Flammable Ester Electrolyte with Boosted Stability Against Li for High-Performance Li Metal Batteries. *Angew. Chem.* **2022**, *134* (41), No. e202206682.

(14) Yamada, Y.; Furukawa, K.; Sodeyama, K.; Kikuchi, K.; Yaegashi, M.; Tateyama, Y.; Yamada, A. Unusual Stability of Acetonitrile-Based Superconcentrated Electrolytes for Fast-Charging Lithium-Ion Batteries. *J. Am. Chem. Soc.* **2014**, *136* (13), 5039−5046.

(15) Chen, S.; Zheng, J.; Mei, D.; Han, K. S.; Engelhard, M. H.; Zhao, W.; Xu, W.; Liu, J.; Zhang, J.-G. High-Voltage Lithium-Metal Batteries Enabled by Localized High-Concentration Electrolytes. *Adv. Mater.* **2018**, *30* (21), 1706102.

(16) Suo, L.; Borodin, O.; Gao, T.; Olguin, M.; Ho, J.; Fan, X.; Luo, C.; Wang, C.; Xu, K. "Water-in-Salt" Electrolyte Enables High-Voltage Aqueous Lithium-Ion Chemistries. *Science* **2015**, *350* (6263), 938−943.

(17) Yamada, Y.; Usui, K.; Sodeyama, K.; Ko, S.; Tateyama, Y.; Yamada, A. Hydrate-Melt Electrolytes for High-Energy-Density Aqueous Batteries. *Nat. Energy* **2016**, *1* (10), 1−9.

(18) Zhang, Q.; De Oliveira Vigier, K.; Royer, S.; Jérôme, F. Deep Eutectic Solvents: Syntheses, Properties and Applications. *Chem. Soc. Rev.* **2012**, *41* (21), 7108−7146.
(19) Boisset, A.; Menne, S.; Jacquemin, J.; Balducci, A.; Anouti, M. Deep Eutectic Solvents Based on N-Methylacetamide and a Lithium Salt as Suitable Electrolytes for Lithium-Ion Batteries. *Phys. Chem. Chem. Phys.* **2013**, *15* (46), 20054−20063.
(20) Liang, Y.; Wu, W.; Li, D.; Wu, H.; Gao, C.; Chen, Z.; Ci, L.; Zhang, J. Highly Stable Lithium Metal Batteries by Regulating the Lithium Nitrate Chemistry with a Modified Eutectic Electrolyte. *Adv. Energy Mater.* **2022**, *12* (47), 2202493.
(21) De Sloovere, D.; Vanpoucke, D. E. P.; Paulus, A.; Joos, B.; Calvi, L.; Vranken, T.; Reekmans, G.; Adriaensens, P.; Eshraghi, N.; Mahmoud, A.; Boschini, F.; Safari, M.; Van Bael, M. K.; Hardy, A. Deep Eutectic Solvents as Nonflammable Electrolytes for Durable Sodium-Ion Batteries. *Adv. Energy Sustainability Res.* **2022**, *3* (3), 2100159.
(22) Li, W.; Liu, W.; Cai, Z.; Huang, B.; Zhong, H.; Mai, Y. Deep Eutectic Solvent with Film-Forming Fluoroethylene Carbonate as a Nonflammable Electrolyte for Lithium Metal Batteries. *J. Energy Storage* **2023**, *68*, 107766.
(23) Li, Y.; Hosaka, T.; Maibach, J.; Johansson, P. Stable Anode Interphase Enabled Use of Protic Electrolytes in Sodium Metal Batteries. *Energy Storage Mater.* **2025**, *82*, 104566.
(24) Kelchtermans, A.-S.; De Sloovere, D.; Mercken, J.; Vranken, T.; Mangione, G.; Joos, B.; Vercruysse, W.; Vandamme, D.; Hamed, H.; Safari, M.; Derveaux, E.; Adriaensens, P.; Van Bael, M. K.; Hardy, A. Superconcentration Strategy Allows Sodium Metal Compatibility in Deep Eutectic Solvents for Sodium-Ion Batteries. *ACS Omega* **2024**, *9* (41), 42343−42352.
(25) Abbott, A. P.; Capper, G.; Davies, L.; Rasheed, R. K.; Tambyrajah, V. Novel solvent properties of choline chloride/urea mixtures. *Chem. Commun.* **2003**, *0* (1), 70−71.
(26) Abbott, A. P.; Boothby, D.; Capper, G.; Davies, D. L.; Rasheed, R. K. Deep Eutectic Solvents Formed between Choline Chloride and Carboxylic Acids: Versatile Alternatives to Ionic Liquids. *J. Am. Chem. Soc.* **2004**, *126* (29), 9142−9147.
(27) Smith, E. L.; Abbott, A. P.; Ryder, K. S. Deep Eutectic Solvents (DESs) and Their Applications. *Chem. Rev.* **2014**, *114* (21), 11060−11082.
(28) Ito, N.; Hosaka, T.; Tatara, R.; Gossage, Z. T.; Komaba, S. Development of Lithium Ion Conducting Liquid: Methylurea-Based Eutectic Electrolytes for Lithium Batteries. *Electrochemistry* **2025**, *93* (2), 027018.
(29) Zhao, L.; Xu, A.; Cheng, Y.; Xu, H.; Xu, L.; Mai, L. A Highly Stable and Non-Flammable Deep Eutectic Electrolyte for High-Performance Lithium Metal Batteries. *Angew. Chem., Int. Ed.* **2024**, *63* (43), No. e202411224.
(30) Wu, W.; Liang, Y.; Li, D.; Bo, Y.; Wu, D.; Ci, L.; Li, M.; Zhang, J. A Competitive Solvation of Ternary Eutectic Electrolytes Tailoring the Electrode/Electrolyte Interphase for Lithium Metal Batteries. *ACS Nano* **2022**, *16* (9), 14558−14568.
(31) Gossage, Z. T.; Hosaka, T.; Matsuyama, T.; Tatara, R.; Komaba, S. Fluorosulfonamide-Type Electrolyte Additives for Long-Life K-Ion Batteries. *J. Mater. Chem. A* **2023**, *11* (2), 914−925.
(32) Ito, N.; Hosaka, T.; Tatara, R.; Gossage, Z. T.; Komaba, S. Development of Lithium Ion Conducting Liquid: Methylurea-Based Eutectic Electrolytes for Lithium Batteries. *Electrochemistry* **2025**, *93*, 027018.
(33) Grimme, S.; Bannwarth, C.; Shushkov, P. A Robust and Accurate Tight-Binding Quantum Chemical Method for Structures, Vibrational Frequencies, and Noncovalent Interactions of Large Molecular Systems Parametrized for All Spd-Block Elements (Z = 1−86). *J. Chem. Theory Comput.* **2017**, *13* (5), 1989−2009.
(34) Bannwarth, C.; Ehlert, S.; Grimme, S. GFN2-xTB—An Accurate and Broadly Parametrized Self-Consistent Tight-Binding Quantum Chemical Method with Multipole Electrostatics and Density-Dependent Dispersion Contributions. *J. Chem. Theory Comput.* **2019**, *15* (3), 1652−1671.
(35) Hutter, J.; Iannuzzi, M.; Schiffmann, F.; VandeVondele, J. Cp2k: Atomistic Simulations of Condensed Matter Systems. *Wiley Interdiscip. Rev.: Comput. Mol. Sci.* **2014**, *4* (1), 15−25.
(36) Yu, Z.; Rudnicki, P. E.; Zhang, Z.; Huang, Z.; Celik, H.; Oyakhire, S. T.; Chen, Y.; Kong, X.; Kim, S. C.; Xiao, X.; Wang, H.; Zheng, Y.; Kamat, G. A.; Kim, M. S.; Bent, S. F.; Qin, J.; Cui, Y.; Bao, Z. Rational Solvent Molecule Tuning for High-Performance Lithium Metal Battery Electrolytes. *Nat. Energy* **2022**, *7* (1), 94−106.
(37) Nurhuda, M.; Perry, C. C.; Addicoat, M. A. Performance of GFN1-xTB for Periodic Optimization of Metal Organic Frameworks. *Phys. Chem. Chem. Phys.* **2022**, *24* (18), 10906−10914.
(38) Wróbel, P.; Eilmes, A. Effects of Me−Solvent Interactions on the Structure and Infrared Spectra of MeTFSI (Me = Li, Na) Solutions in Carbonate Solvents—A Test of the GFN2-xTB Approach in Molecular Dynamics Simulations. *Molecules* **2023**, *28* (18), 6736.
(39) Pokora, M.; Goclon, J.; Margraf, J.; Panosetti, C.; Samtsevych, A.; Paneth, P. Low-Cost Periodic Calculations of Metal-Organic Frameworks: A GFN1-xTB Perspective. *ChemPhysChem* **2025**, *26* (14), No. e202500081.
(40) Martínez, L.; Andrade, R.; Birgin, E. G.; Martínez, J. M. PACKMOL: A package for building initial configurations for molecular dynamics simulations. *J. Comput. Chem.* **2009**, *30* (13), 2157−2164.
(41) Nosé, S. A Unified Formulation of the Constant Temperature Molecular Dynamics Methods. *J. Chem. Phys.* **1984**, *81* (1), 511−519.
(42) Hoover, W. G. Canonical Dynamics: Equilibrium Phase-Space Distributions. *Phys. Rev. A* **1985**, *31* (3), 1695−1697.
(43) Evans, D. J.; Holian, B. L. The Nose−Hoover Thermostat. *J. Chem. Phys.* **1985**, *83* (8), 4069−4074.
(44) Humphrey, W.; Dalke, A.; Schulten, K. VMD: Visual Molecular Dynamics. *J. Mol. Graphics* **1996**, *14* (1), 33−38.
(45) Adam, G.; Gibbs, J. H. On the Temperature Dependence of Cooperative Relaxation Properties in Glass-Forming Liquids. *J. Chem. Phys.* **1965**, *43* (1), 139−146.
(46) Angell, C. A. Formation of Glasses from Liquids and Biopolymers. *Science* **1995**, *267* (5206), 1924−1935.
(47) Han, S.-D.; Sommer, R. D.; Boyle, P. D.; Zhou, Z.-B.; Young, V. G.; Borodin, O.; Henderson, W. A. Electrolyte Solvation and Ionic Association: Part IX. Structures and Raman Spectroscopic Characterization of LiFSI Solvates. *J. Electrochem. Soc.* **2022**, *169* (11), 110544.
(48) Lemon, M. T.; Jones, M. S.; Stansbury, J. W. Hydrogen Bonding Interactions in Methacrylate Monomers and Polymers. *J. Biomed. Mater. Res., Part A* **2007**, *83A* (3), 734−746.
(49) Yoshida, K.; Nakamura, M.; Kazue, Y.; Tachikawa, N.; Tsuzuki, S.; Seki, S.; Dokko, K.; Watanabe, M. Oxidative-Stability Enhancement and Charge Transport Mechanism in Glyme−Lithium Salt Equimolar Complexes. *J. Am. Chem. Soc.* **2011**, *133* (33), 13121−13129.
(50) Yamada, Y.; Yamada, A. Review—Superconcentrated Electrolytes for Lithium Batteries. *J. Electrochem. Soc.* **2015**, *162* (14), A2406−A2423.
(51) Adams, B. D.; Zheng, J.; Ren, X.; Xu, W.; Zhang, J.-G. Accurate Determination of Coulombic Efficiency for Lithium Metal Anodes and Lithium Metal Batteries. *Adv. Energy Mater.* **2018**, *8* (7), 1702097.
(52) Brandt, A.; Pires, J.; Anouti, M.; Balducci, A. An Investigation about the Cycling Stability of Supercapacitors Containing Protic Ionic Liquids as Electrolyte Components. *Electrochim. Acta* **2013**, *108*, 226−231.
(53) Qian, J.; Henderson, W. A.; Xu, W.; Bhattacharya, P.; Engelhard, M.; Borodin, O.; Zhang, J.-G. High Rate and Stable Cycling of Lithium Metal Anode. *Nat. Commun.* **2015**, *6* (1), 6362.
(54) Yamada, Y.; Furukawa, K.; Sodeyama, K.; Kikuchi, K.; Yaegashi, M.; Tateyama, Y.; Yamada, A. Unusual Stability of Acetonitrile-Based Superconcentrated Electrolytes for Fast-Charging Lithium-Ion Batteries. *J. Am. Chem. Soc.* **2014**, *136* (13), 5039−5046.

https://doi.org/10.1021/acsaem.5c02275
ACS Appl. Energy Mater. XXXX, XXX, XXX−XXX